Published in final edited form as:
J Magn Reson Imaging. 2015 January ; 41(1): 102–109. doi:10.1002/jmri.24550.

White Matter Lesion Load Is Associated With Resting State Functional MRI Activity and Amyloid PET but not FDG in Mild Cognitive Impairment and Early Alzheimer's Disease Patients

Yongxia Zhou, PhD[1,2,*], **Fang Yu, MD**[3,4], **Timothy Q. Duong, PhD**[3,4], and **the Alzheimer's Disease Neuroimaging Initiative**

[1]Radiology/Center for Biomedical Imaging, New York University School of Medicine, New York, New York, USA

[2]Radiology, University of Pennsylvania, Philadelphia, Pennsylvania, USA

[3]Research Imaging Institute, Departments of Ophthalmology, Radiology, Physiology, University of Texas Health Science Center, San Antonio, Texas, USA

[4]South Texas Veterans Health Care System, Department of Veterans Affairs, San Antonio, Texas, USA

Abstract

Purpose—To quantify and investigate the interactions between multimodal MRI/positron emission tomography (PET) imaging metrics in elderly patients with early Alzheimer's disease (AD), mild cognitive impairment (MCI) and healthy controls.

Materials and Methods—Thirteen early AD, 17 MCI patients, and 14 age-matched healthy aging controls from the Alzheimer's Disease Neuroimaging Initiative database were selected based on availability of data. Default mode network (DMN) functional connectivity and fractional amplitude of low frequency fluctuation (fALFF) were obtained for resting state functional MRI (RS-fMRI). White matter lesion load (WMLL) was quantified from MRI T2-weighted FLAIR images. Amyloid deposition with PET [^{18}F]-Florbetapir tracer and metabolism of glucose by means of [^{18}F]-fluoro-2-deoxyglucose (FDG) images were quantified using ratio of standard uptake values (rSUV).

Results—Whole-brain WMLL and amyloid deposition were significantly higher ($P < 0.005$) in MCI and AD patients compared with controls. RS-fMRI results showed significantly reduced (corrected $P < 0.05$) DMN connectiv ity and altered fALFF activity in both MCI and AD groups. FDG uptake results showed hypometabolism in AD and MCI patients compared with controls.

*Address reprint requests to: Y.Z., Center for Biomedical Imaging, Department of Radiology, New York University School of Medicine 660 First Avenue, 4th Floor, New York, NY 10016. yongxia.zhou@yahoo.com, zhouyong@mail.med.upenn.edu.

Data used in preparation of this article were obtained from the Alzheimer's Disease Neuroimaging Initiative (ADNI) database (adni.loni.ucla.edu). As such, the investigators within the ADNI contributed to the design and implementation of ADNI and/or provided data but did not participate in analysis or writing of this report. A complete listing of ADNI investigators can be found at: http://adni.loni.ucla.edu/wpcontent/uploads/how_to_apply/ADNI_Acknowledgement_List.pdf.

Correlations ($P < 0.05$) were found between WMLL and amyloid load, FDG uptake and amyloid load, as well as between amyloid load (rSUV) and fALFF.

Conclusion—Our quantitative results of four MRI and PET imaging metrics (fALFF/DMN, WMLL, amyloid, and FDG rSUV values) agree with published values. Signifi-cant correlations between MRI metrics, including WMLL/ functional activity and PET amyloid load suggest the potential of MRI and PET-based biomarkers for early detection of AD.

Keywords

white matter lesion; amyloid; resting state-fMRI; Alzheimer disease; fractional amplitude at low frequency fluctuation; default mode network

White matter (WM) lesion, detected as WM hyper-intensities (WMH) on MRI T2-weighted images, may represent microvascular ischemic and/or demyelinating changes (1) and in which cases they can be considered a marker for cerebrovascular disease (CVD) (2,3). In the elderly population, WM lesion is believed to be potential risk factor for memory and cognitive impairment (4). WMH have been found to be associated with an increased incidence of dementia (5), as well as the development of WM microstructural changes in the presymptomatic stage of disease (6). Using diffusion tensor imaging (DTI), age-related WM degeneration (i.e., fractional anisotropy and diffusivity) has been identified, particularly in the prefrontal cortex and splenium of corpus callosum (7). DTI tractography of the posterior cingulate and hippocampal WM regions in mild cognitive impairment (MCI) and early Alzheimer's disease (AD) demonstrate reduced fiber tract numbers as well, consistent with reduced functional connectivity noted on fMRI (8). Negative correlations between WMH lesions and fMRI BOLD signals in elderly individuals performing episodic memory or finger tapping tasks have been reported in the prefrontal and parietal regions (9,10). Greater WMH lesion burden were also found in elderly individuals with microbleeds based on MRI T2* gradient echo and susceptibility weighted images, suggesting a possible microhemorrhage contribution to WMH in aging (11). These results suggest that there are WM micro-structural and cerebrovascular disruptions in both elderly and demented subjects. However, the threshold separating WM lesion burden in the normal elderly population and dementia/AD patients has yet to be determined.

The pathological hallmarks of early AD are amyloid plaques and mis-folded tau tangles (12). A significant relationship between the composite AD pathological score at autopsy and white matter disease score from T2-weighted MRI images was found among a cohort of elderly subjects (13). Amyloid plaque distribution patterns have been found to colocalize with resting state (RS)-fMRI core hub regions such as the default mode network (DMN), even before the clinical onset of disease (14). Furthermore, hypometabolism based on Fluoro-2-deoxyglucose ([^{18}F]-FDG) PET, which is considered a marker of neuronal dysfunction, has been shown to be a prominent feature in early AD, particularly in the posterior parietal and cingulate regions (15). Although the extracellular amyloid deposition is not directly correlated with detectable vascular injury (i.e., cerebral amyloid angiopathy, CAA) (16), its association with white matter damage and RS-fMRI changes in different stages of dementia needs to be further examined (17).

Prior studies have shown that the hazard ratio increases linearly with the number of risk factors, including CVD and amyloid burden (18). This points to the possibility that earlier identification and modification of such risk factors may lead to clinical prevention and even treatment of AD dementia. Using fractional amplitude of low frequency fluctuation (fALFF) technique to detect neuronal activity at resting state is relatively new. The fALFF technique works by filtering, scaling, and normalization to control for physiological/random noise, ventricular contamination and global individual differences to enhance baseline functional activity (19). The specific aims of this study are to (i) compare the WM lesion volume, amyloid burden, FDG uptake, and RS-fMRI changes (e.g., fALFF) in patients with early AD, MCI and healthy controls; and (ii) investigate the interactions between these MRI/PET imaging metrics.

METHODS

Subjects

Thirteen early AD patients (age: 76.2 ± 8.4 years, Mini-Mental State Examination [MMSE] score < 24), 17 patients with MCI (age: 76.7 ± 5.5 years, MMSE: 24–28), and 14 age-matched healthy controls (age: 76.3 6 8.25 years, MMSE > 28) from the AD neuroimaging initiative (ADNI) database (http://adni.loni.ucla.edu) were used in this study. Data were selected based on age ranges of subjects as well as availability of four imaging modal ities for the same subject during the period of October 2010 to August 2013. Demographic information of subjects is summarized in Table 1.

MR/PET Imaging

ADNI—Data used in the preparation of this article were obtained from the Alzheimer's Disease Neuroimaging Initiative (ADNI) database (http:/www.adni.loni.ucla. edu). The primary goal of ADNI has been to test whether serial MRI, positron emission tomography (PET), other biological markers, and clinical and neuropsychological assessment can be combined to measure the progression of mild cognitive impairment (MCI) and early Alzheimer's disease (AD). ADNI is the result of efforts of many co-investigators from a broad range of academic institutions and private corporations, and subjects have been recruited from over 50 sites across the United States and Canada. For up-to-date information, see www.adni-info.org.

Imaging Data—RS-fMRI (repetition time/echo time [TR/TE] = 3000/30 ms, flip angle = 80° , 3.3 mm isotropic spatial resolution with 48 slices and 140 volumes), T1-MPRAGE (acquired sagittally using volumetric 3D MPRAGE with 0.94 ×.94 mm^2 in-plane spatial resolution, 1.2 mm slice thickness with matrix size of 256 × 256 and 166 slices), and T2-weighted axial fluid attenuated inversion recovery (FLAIR) images (TR/TE = 9000/90ms, flip angle = 90° , 0.86 ×.86 mm^2 in-plane spatial resolution, 5 mm thick and 35 slices) were obtained with 3T MRI units at multiple ADNI centers with standardized imaging protocols across sites and platforms. In addition, [^{18}F]-Florbetapir amyloid PET images from the same subject with standard ADNI protocol were acquired for each subject (1.02 ×.02 mm^2 in-plane spatial resolution, 2 mm thick, and 109 slices covering the whole brain). [^{18}F]-FDG PET images (scanned at the same day as [^{18}F]-Florbetapir with standard ADNI protocol,

reconstructed with 2 2 mm^2 in-plane spatial resolution, 3.27 mm thick, and 47 slices covering the whole brain) were obtained for each subject as well. The time durations between PET and MRI scans were less than 3 months for the same subject.

Data Analysis

Default mode network (DMN) based on RS-fMRI was generated with seeds placed in both medial prefrontal cortex (MPFC) and posterior cingulate cortex (PCC) core areas (20). These two representative regions (MPFC and PCC) were selected for further analysis based on their roles in memory encoding and consolidation, self-relevance and social functions, which are often disrupted in patients with AD (14). This combined seed-based connectivity has been used for automatic DMN pattern detection with high specificity (21). In addition, fALFF was obtained with adapted scripts in FSL (http://fsl.fmrib.ox.ac.uk/fsl, version 4.1.2). This involved summarizing over 0.005–0.1 Hz frequency band, followed by scaling to the whole band in the frequency domain to remove white and physiological noise after preprocessing steps (19).

WM lesions, indicated as hyperintensities on the FLAIR images, were segmented semi-automatically (manual outlining with white matter intensity constraints) using FireVoxel software for each subject (22). The whole brain white matter lesion load (WMLL) was obtained as the volume (in units of milliliter, mL) of the hyper-intense (≥ mean+2.5 standard deviation) voxels in WM. Then the lesion map generated from the FLAIR images was co-registered to MPRAGE data of each subject and normalized to the Montreal Neurological Institute (MNI) 2mm standard space in FSL using a nonlinear warping algorithm. Finally, the lesion probability map (LPM) was generated by averaging the binarized normalized lesion maps within each group.

Similar to RS-fMRI data preprocessing (19), [^{18}F]-Florbetapir and [^{18}F]-FDG PET images for quantifying amyloid load and glucose uptake values were co-registered to the MPRAGE images and warped to the common MNI space using the FSL FNIRT command. Cortical and subcortical parcellations in 113 regions of interest (ROI), including regions of the MPFC, PCC, and cerebellum (for PET scaling) in the FSL template space were used to calculate PET regional standard uptake values (rSUV). Averaged rSUV in each region was normalized with the average SUV of gray matter of the cerebellum.

Statistical Analysis

Voxel-wise FSL easythresh command with multi-comparison corrections at the cluster level were performed using Gaussian random field theory (minimum, $z > 2.3$; cluster significance, $P < 0.05$, corrected) for RS-fMRI within and between group differences. Correlational analyses were performed between WMLL, amyloid burden, glucose metabolism, and RS-fMRI by using both Pearson and Spearman rank correlation methods.

RESULTS

Based on the FLAIR images, a varying degree of periventricular and frontal white matter lesions in AD and MCI patients as well as controls were identified. LPM (lesion distribution) is shown in Figure 1A1–3 for the control, MCI and AD groups respectively.

PET amyloid uptake image is shown in Figure 1B1–3 for average normalized amyloid load in three groups as well, with the most significant uptake noted in the AD group. Quantitative whole brain WMLL was significantly higher in patients with MCI (12.88 ± 7.47 mL) and AD (13.16 ± 5.12 mL) than controls (5.15 ± 2.41 mL) (Fig. 2), both with $P < 0.005$.

Quantitative global cerebral cortex amyloid uptake (i.e., rSUV) showed a higher-degree of amyloid deposition in patients with MCI (0.42 ± 0.15) and early AD (1.58 ± 0.20) compared with controls (0.15 ± 0.12), both with $P < 0.001$ (Fig. 3A). Regional normalized uptake values also demonstrated significantly higher uptake values in MCI and AD, with the highest degree in the AD group with $P < 0.001$, including the PCC ($P < 0.005$) (1.15 ± 0.21 in controls, 1.56 ± 0.33 in MCI and 1.77 ± 0.41 in AD) (Fig. 3B) and MPFC ($P < 0.005$) (1.20 ± 0.35 in controls, 1.66 ± 0.35 in MCI and 1.82 6 0.27 in AD) (Fig. 3C). However, there was no significant difference in the amyloid uptake between the patients with early AD compared with MCI in either the entire cortex (*P* 0.07), (*P* 0.07), or MPFC (*P* 0.39) (Fig. 3).

In terms of RS-fMRI, there was significantly reduced DMN connectivity in the MPFC as well as reduced fALFF activity in the temporal cortex in the MCI group compared with controls (minimum $z > 2.3$; corrected cluster significance $P < 0.05$) (Fig. 4A). Reduced DMN connectivity was also noted in early AD patients compared with MCI patients, but not statistically signifi- cant ($P > 0.05$). The fALFF was reduced in the temporal cortex but increased in the parietal cortex in AD compared with MCI patients (minimum $z > 2.3$; corrected cluster significance $P < 0.05$) (Fig. 4B).

A significant correlation was found between WMLL and amyloid load averaged over the whole cerebral cortex in all three groups (Pearson $r = 0.46$, *P* 0.015; Spearman rank $r = 0.46$, $P = 0.013$) (Fig. 5). There were also significant correlations between WMLL and amyloid load in the PCC (Pearson *r* 0.4, *P* 0.04; Spear-man rank $r = 0.43$, *P* 0.023), as well as between the WMLL and MPFC amyloid load (Person $r = 0.45$, $P = 0.018$; Spearman rank $r = 0.43$, $P = 0.023$) (Fig.5).

A significant correlation was found between WMLL and DMN connectivity strength (r 0.56; P 0.02), as well as between WMLL and fALFF activity values (r = 0.63; $P = 0.01$) (Fig. 6A) in MCI patients. Mean-while, in AD patients, a marginal interregional correlation exists between the RS-fMRI fALFF activity value averaged over the reduced and increased regions (r = 0.46; $P = 0.11$). A significant correlation was found between amyloid load of the whole cerebral cortex and lower fALFF activity value in AD patients (r = 0.64; *P* 0.046) (Fig. 6B).

Regarding the FDG uptake, there was significantly lower cerebral FDG rSUV in MCI and AD patients compared to controls ($P = 0.002$) (Fig. 7A). However, there was no significant difference between MCI and AD patients ($P = 0.71$). A negative correlation between FDG uptake and amyloid load was noted in the 3 groups (r = 0.57; $P = 0.0006$) (Fig. 7B). FDG rSUV was not correlated significantly with either WMLL or RS-fMRI activity.

The spatial correspondences, various comparisons, and associations of multiple imaging features are illustrated in Figure 8, with the dynamic correspondence between amyloid load,

FDG uptake, WMLL, and RS-fMRI fALFF metrics at different stages of disease (from control to MCI and early AD) summarized in Figure 8B.

DISCUSSION

We found a typical peri-ventricular and frontal WM lesion distribution in MCI and AD patients (21,23,24). Our comparison results also showed significantly elevated global WMLL in MCI and AD patients compared with controls. Meanwhile, these values were not sig nificantly different for early AD compared with MCI patients. A recent study indicated that based on global and temporal WM lesions alone, differentiation between stages of cognitive impairment, as well as prediction of progression to dementia (including AD), may be achieved (25). Our results support the notion that WM lesions were detectable at a prodromal stage and may provide additional insights into early AD detection.

Our global cerebral, regional PCC, and MPFC quantitative amyloid load (i.e., rSUV) were similar to those published within the same age range for MCI and AD (26). We found the difference between controls and MCI was more prominent in the MPFC than the PCC. However, the rSUV difference between MCI and AD was slightly more prominent (but not significantly different) in the PCC than in the MPFC, suggesting different spatiotemporal profiles of amyloid burden. Joie et al found that regional rSUV differences between controls and probable AD (a mixture of MCI and early AD population) were similar in the PCC and MPFC (27). With a larger study population, Nordberg et al reported significant differences in these two regions between controls and MCI as well as between MCI and AD (28). Our observation of progression of amyloid load is consistent with the current view that amyloid accumulation in MCI patients begins to plateau while progressing to early AD (29).

The moderate correlation between WMLL and amyloid load in controls as well as affected populations suggests a possible link between microvascular damage and amyloid pathology at the early stages of Alzheimer's disease (i.e., MCI and early AD). However, the spatial distribution pattern of WMLL (periventricular and frontal WM) and amyloid load (predominantly in MPFC and PCC cortical areas) were different, suggesting these two regions may be distinctly involved at different stages of dementia. A significant negative correlation was found between FDG uptake and amyloid load in the three aging populations, indicating a correspondence between amyloid pathology and metabolism (e.g., hypometabolism in MCI and AD patients) at the early stages of Alzheimer's disease as well. The different temporal trajectories of FDG and Florbetapir has been reported before (29), and it might be possible that at early stages especially at MCI and AD, these two biomarkers co-occur and thus producing significant correlations. However, we also noted the differences between these two tracers given that FDG is more sensitive in diagnosing AD (from mild to severe) while Florbetapir is used for pathological specification and prediction of disease progression, particularly in early AD (30).

The RS-fMRI results showed reduced functional connectivity in the DMN MPFC region and reduced functional activity by means of fALFF in the temporal region in MCI patients compared with controls. The fALFF was also reduced in the temporal region in AD compared with MCI patients, but increased in the parietal region. As may be expected, we

found reduced neuronal activity in the temporal cortex, where AD patients often demonstrate atrophy and degeneration (31). The increased parietal fALFF in AD suggests a compensatory mechanism for the reduced temporal fALFF based on the marginal correlation between fALFF values of these two regions. The disruption of high-frequency components, such as those involved in memory encoding or retrieval tasks in the parietal regions (32), could also lead to the observed increased fALFF. Our findings were in-line with the literature, suggesting a functional compensatory and neuroplasticity mechanism in response to the accumulation of amyloid plaques in early AD (32). The mild negative correlation between amyloid burden and fMRI activity in AD patients noted in our study appears to suggest a causative effect of amyloid pathology on disease progression. Similarly, recent studies have reported negative correlations between whole-brain (33) as well as regional fMRI connectivity and amyloid burden (34).

The negative correlation between increased WMLL and RS-fMRI abnormalities only in MCI patients suggests WM lesions may play an important role in cognitive decline secondary to decreased functional connectivity (on DMN) and reduced spontaneous activity (fALFF) in the prodromal stage of dementia. On the other hand, the negative correlation between increased amyloid load and RS-fMRI abnormalities only in AD patients suggests amyloid deposition may lead to a reduction in spontaneous activity reflected by fALFF as the disease progresses. The fact that WMLL and amyloid load had distinctively separate associations with the functional deficits reflected on fMRI, suggests different sensitivities of each imaging metric at different stages of cognitive decline. In essence, the functional deficits observed in the MCI stage coincide with the WM lesions, whereas once the disease progresses to the early AD stage, the amyloid burden demonstrates a more direct relationship with neuronal activity deficits. Several studies have found correlations between amyloid load and cognitive decline, more prominently at cognitively normal and earlier MCI stages than later MCI and early AD stages (35,36), based on either [^{11}C]-PIB or [^{18}F]-Florbetapir PET ligands. The difference between our observation and the previously published articles (35,36) may derive from the fact that we correlated amyloid load directly with fMRI connectivity or activity metrics instead of cognitive function measures (i.e., ADAS-cog and CDR scores). Additionally it is possible that at least in some patients, neurological deficits detected by cognitive neuroimaging results might present in a different time frame from the manifestations of mild cognitive functional symptoms, possibly due to cognitive reserves against brain pathology or age-related changes (37), as suggested by PET-FDG results (30).

Limitations of our study include relatively small number of subjects as well as nonsimultaneous acquisitions of PET and MRI images. Partial correlation could be further investigated to tease out any age and gender confounding effects that might be different for each variable in the correlational analysis. As there were different factors contributing to the WMLL in the aging population (38), further longitudinal follow-up is needed to determine to what degree the amyloid pathology and/or other pathological factors (e.g., axonal degeneration) might cause or co-occur with WM lesions in MCI and AD. Although we hoped to identify early imaging biomarkers based on in vivo imaging findings, other genetic/immune system and non-amyloid pathways may contribute to the neuro-degenerative process as well (39).

In conclusion, our quantitative analyses implicated the potential of MRI and PET-based biomarkers for early detection of AD. Of particular relevance, the correlational imaging results of vascular, functional and pathological metrics appear to support the current strategies of AD prevention through early identification of risk factors such as hypertension and hyper-cholesterolemia that may lead to amyloidosis and WM hyperintensities (40).

ACKNOWLEDGMENTS

Data collection and sharing for this project was funded by the Alzheimer's Disease Neuroimaging Initi ative (ADNI). ADNI is funded by the National Institute on Aging, the National Institute of Biomedical Imaging and Bioengineering, and through generous contributions from the following: Abbott; Alzheimer's Association; Alzheimer's Drug Discovery Foundation; Amorfix Life Sciences Ltd.; AstraZeneca; Bayer HealthCare; BioClinica, Inc.; Biogen Idec Inc.; Bristol-Myers Squibb Company; Eisai Inc.; Elan Pharmaceuticals Inc.; Eli Lilly and Company; F. Hoffmann-La Roche Ltd and its affiliated company Genentech, Inc.; GE Healthcare; Innogenetics, N.V.; IXICO Ltd.; Janssen Alzheimer Immunotherapy Research & Development, LLC.; Johnson & Johnson Pharmaceutical Research & Development LLC.; Medpace, Inc.; Merck & Co., Inc.; Meso Scale Diagnostics, LLC.; Novartis Pharmaceuticals Corporation; Pfizer Inc.; Servier; Synarc Inc.; and Takeda Pharmaceutical Company. The Canadian Institutes of Health Research is providing funds to support ADNI clinical sites in Canada. Private sector contributions are facilitated by the Foundation for the National Institutes of Health (www.fnih.org). The grantee organization is the Northern California Institute for Research and Education, and the study is coordinated by the Alzheimer's Disease Cooperative Study at the University of California, San Diego. ADNI data are disseminated by the Laboratory for Neuro Imaging at the University of California, Los Angeles.

Contract grant sponsor: National Institutes of Health; Contract grant numbers: U01 AG024904, P30 AG010129, K01 AG030514.

REFERENCES

1. Chui HC. Vascular cognitive impairment: today and tomorrow. Alzheimers Dement. 2006; 2:185–194. [PubMed: 19595882]
2. Debette S, Markus HS. The clinical importance of white matter hyperintensities on brain magnetic resonance imaging: systematic review and meta-analysis. BMJ. 2010; 341:c3666. [PubMed: 20660506]
3. Wardlaw JM, Smith EE, Biessels GJ, et al. Neuroimaging standards for research into small vessel disease and its contribution to ageing and neurodegeneration. Lancet Neurol. 2013; 12:822–838. [PubMed: 23867200]
4. Geppert AM, Wroblewska KA, Przedpelska-Ober EM. Greater frequency of subcortical lesions in severely demented patients with early onset Alzheimer's disease. Alzheimers Dement. 2007; 3:54–57. [PubMed: 19595917]
5. Brickman AM, Provenzano FA, Muraskin J, et al. Regional white matter hyperintensity volume, not hippocampal atrophy, predicts incident Alzheimer disease in the community. Arch Neurol. 2012; 69:1621–1627. [PubMed: 22945686]
6. Ryan NS, Keihaninejad S, Shakespeare TJ, et al. Magnetic resonance imaging evidence for presymptomatic change in thalamus and caudate in familial Alzheimer's disease. Brain. 2011; 136:1399–1414. [PubMed: 23539189]
7. Salat DH, Tuch DS, Greve DN, et al. Age-related alterations in white matter microstructure measured by diffusion tensor imaging. Neurobiol Aging. 2005; 26:1215–1227. [PubMed: 15917106]
8. Zhou Y, Dougherty JH Jr, Hubner KF, Bai B, Cannon RL, Hutson RK. Abnormal connectivity in the posterior cingulate and hippocampus in early Alzheimer's disease and mild cognitive impairment. Alzheimers Dement. 2008; 4:265–270. [PubMed: 18631977]
9. Nordahl CW, Ranganath C, Yonelinas AP, DeCarli C, Fletcher E, Jagust WJ. White matter changes compromise prefrontal cortex function in healthy elderly individuals. J Cogn Neurosci. 2006; 18:418–429. [PubMed: 16513006]

10. Patel MJ, Boada FE, Price JC, et al. Association of small vessel ischemic white matter changes with BOLD fMRI imaging in the elderly. Psychiatry Res. 2012; 204:117–122. [PubMed: 23131524]
11. Whitwell JL, Jack CR Jr, Duffy JR, et al. Microbleeds in the logo-penic variant of primary progressive aphasia. Alzheimers Dement. 2013; 9:1–5. [PubMed: 23305821]
12. Braak H, Braak E. Neuropathological stageing of Alzheimer-related changes. Acta Neuropathol. 1991; 82:239–259. [PubMed: 1759558]
13. Moghekar A, Kraut M, Elkins W, et al. Cerebral white matter disease is associated with Alzheimer pathology in a prospective cohort. Alzheimers Dement. 2012; 8(Suppl):S71–S77. [PubMed: 23021624]
14. Buckner RL, Snyder AZ, Shannon BJ, et al. Molecular, structural, and functional characterization of Alzheimer's disease: evidence for a relationship between default activity, amyloid, and memory. J Neurosci. 2005; 25:7709–7717. [PubMed: 16120771]
15. Silverman DH, Small GW, Chang CY, et al. Positron emission tomography in evaluation of dementia: regional brain metabolism and long-term outcome. JAMA. 2001; 286:2120–2127. [PubMed: 11694153]
16. Takada LT, Camiz P, Grinberg LT, da Costa Leite C. Non-inflammatory cerebral amyloid angiopathy as a cause of rapidly progressive dementia - a case study. Dement Neuropsychol. 2009; 3:352–257.
17. Zhou Y, Ge Y, De Leon M. White matter lesion load is associated with resting state fMRI activity in mild cognitive impairment patients. Alzheimers Dement. 2012; 8:535–536.
18. Reed BR, Marchant NL, Jagust WJ, Decarli C, Mack W, Chui HC. Coronary risk corrlates with cerebral amyloid deposition. Neurobiol Aging. 2012; 33:1979–1987. [PubMed: 22078485]
19. Zhou Y, Lui YW, Zuo X-N, et al. Characterization of thalamocortical association using amplitude and connectivity of fMRI in mild traumatic brain injury. J Magn Reson Imaging. 2013 (in press).
20. Zhou Y, Milham MP, Lui YW, et al. Default-mode network disruption in mild traumatic brain injury. Radiology. 2012; 265:882–892. [PubMed: 23175546]
21. Greicius MD, Krasnow B, Reiss AL, Menon V. Functional connectivity in the resting brain: a network analysis of the default mode hypothesis. Proc Natl Acad Sci U S A. 2004; 101:4637–4642. [PubMed: 15070770]
22. Mikheev A, Nevsky G, Govindan S, Grossman R, Rusinek H. Fully automatic segmentation of the brain from T1-weighted MRI using Bridge Burner algorithm. J Magn Reson Imaging. 2008; 27:1235–1241. [PubMed: 18504741]
23. Damian MS, Schilling G, Bachmann G, Simon C, Stoppler S, Dorndorf W. White matter lesions and cognitive deficits: relevance of lesion pattern? Acta Neurol Scand. 1994; 90:430–436. [PubMed: 7892763]
24. Bendfeldt K, Blumhagen JO, Egger H, et al. Spatiotemporal distribution pattern of white matter lesion volumes and their association with regional grey matter volume reductions in relapsingremitting multiple sclerosis. Hum Brain Mapp. 2010; 31:1542–1555. [PubMed: 20108225]
25. Mortamais M, Reynes C, Brickman AM, et al. Spatial distribution of cerebral white matter lesions predicts progression to mild cognitive impairment and dementia. PloS One. 2013; 8:e56972. [PubMed: 23457645]
26. Huang KL, Lin KJ, Hsiao IT, et al. Regional amyloid deposition in amnestic mild cognitive impairment and Alzheimer's disease evaluated by [(18)F]AV-45 positron emission tomography in Chinese population. PloS One. 2013; 8:e58974. [PubMed: 23516589]
27. La Joie R, Perrotin A, Barre L, et al. Region-specific hierarchy between atrophy, hypometabolism, and β-amyloid (Aβ) load in Alzheimer's disease dementia. J Neurosci. 2012; 32:16265–16273. [PubMed: 23152610]
28. Nordberg A, Carter SF, Rinne J, et al. A European multicentre PET study of fibrillar amyloid in Alzheimer's disease. Eur J Nucl Med Mol Imaging. 2013; 40:104–114. [PubMed: 22961445]
29. Jack CR Jr, Knopman DS, Jagust WJ, et al. Tracking pathophysiological processes in Alzheimer's disease: an updated hypothetical model of dynamic biomarkers. Lancet Neurol. 2013; 12:207–216. [PubMed: 23332364]

30. Mosconi L, Berti V, Glodzik L, Pupi A, De Santi S, de Leon MJ. Pre-clinical detection of Alzheimer's disease using FDG-PET, with or without amyloid imaging. J Alzheimers Dis. 2010; 20:843–854. [PubMed: 20182025]

31. Rusinek H, Endo Y, De Santi S, et al. Atrophy rate in medial temporal lobe during progression of Alzheimer disease. Neurology. 2004; 63:2354–2359. [PubMed: 15623699]

32. Sperling RA, Johnson KA, Doraiswamy PM, et al. Amyloid deposition detected with florbetapir F 18 ((18)F-AV-45) is related to lower episodic memory performance in clinically normal older individuals. Neurobiol Aging. 2013; 34:822–831. [PubMed: 22878163]

33. Drzezga A, Becker JA, Van Dijk KRA, et al. Neuronal dysfunction and disconnection of cortical hubs in non-demented subjects with elevated amyloid burden. Brain. 2011; 134:1635–1646. [PubMed: 21490054]

34. Sheline YI, Raichle ME, Snyder AZ, et al. Amyloid plaques disrupt resting state default mode network connectivity in cognitively normal elderly. Bio Psychiatry. 2010; 67:584–587. [PubMed: 19833321]

35. Doraiswamy PM, Sperling RA, Coleman RE, et al. Amyloid-beta assessed by florbetapir F 18 PET and 18-month cognitive decline: a multicenter study. Neurology. 2012; 79:1636–1644. [PubMed: 22786606]

36. Storandt M, Mintun MA, Head D, Morris JC. Cognitive decline and brain volume loss as signatures of cerebral amyloid-beta peptide deposition identified with Pittsburgh compound B: cognitive decline associated with Abeta deposition. Arch Neurol. 2009; 66:1476–1481. [PubMed: 20008651]

37. Stern Y. Cognitive reserve in ageing and Alzheimer's disease. Lancet Neurol. 2012; 11:1006–1012. [PubMed: 23079557]

38. Kling MA, Trojanowski JQ, Wolk DA, Lee VM, Arnold SE. Vascular disease and dementias: paradigm shifts to drive research in new directions. Alzheimers Dement. 2013; 9:76–92. [PubMed: 23183137]

39. Herrup K, Carrillo MC, Schenk D, et al. Beyond amyloid: getting real about nonamyloid targets in Alzheimer's disease. Alzheimers Dement. 2013; 9:452–458. [PubMed: 23809366]

40. Kling MA, Trojanowski JQ, Wolk DA, Lee VM, Arnold SE. Vascular disease and dementias: paradigm shifts to drive research in new directions. Alzheimers Dement. 2013; 9:76–92. [PubMed: 23183137]

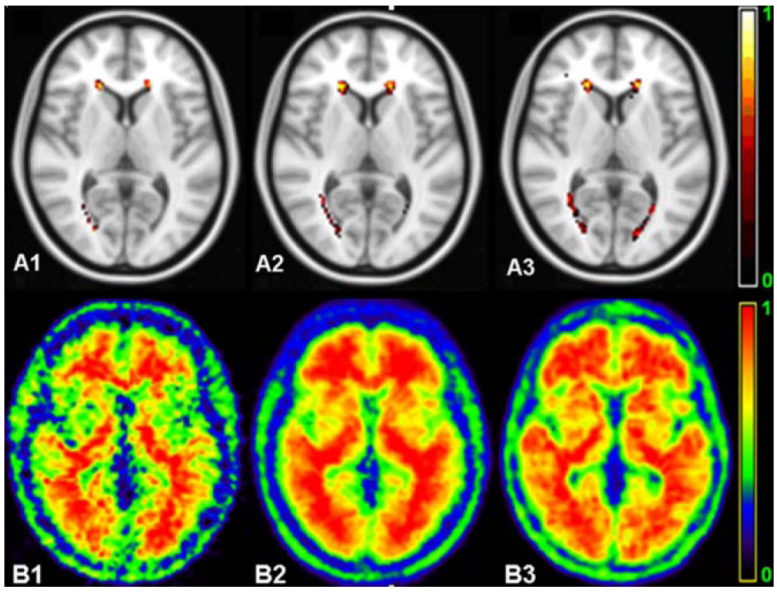

Figure 1.

A: Representative axial slice of lesion probability map (LPM) in each group based on MRI T2-FLAIR images showed a peri-ventricular WM lesion distribution. Compared with controls (A1), LPM in MCI (A2), and AD (A3) groups showed significantly increased WM lesions in especially the left periventricular WM around the occipital horn and frontal WM. B: Amyloid imaging using PET [^{18}F]-Florbetapir tracer in the normal control (B1), MCI (B2), and AD (B3) subjects showed increased amyloid deposition patterns in MCI patients in medial frontal and parietal regions; and increased uptake in almost the whole brain in AD patients. Amyloid deposition was averaged across subjects in each group after normalizing with the maximal value individually.

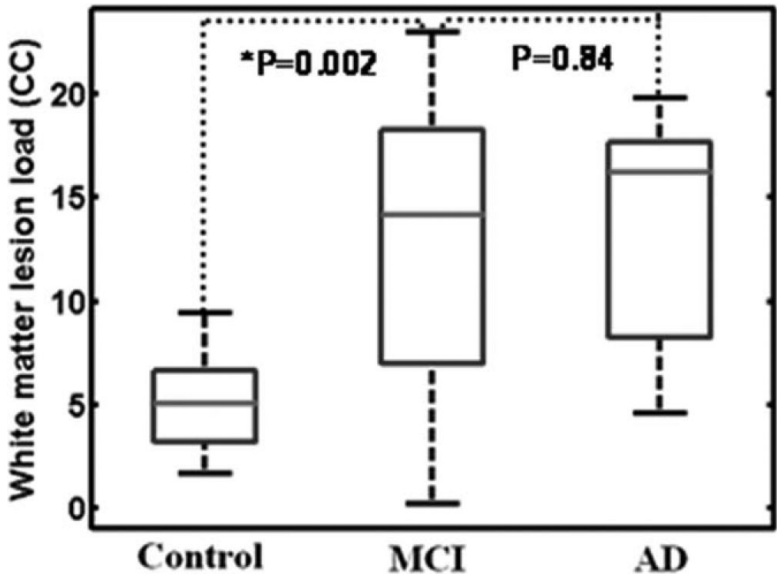

Figure 2.

Compared with controls, there was significantly increased whole brain white matter lesion load (WMLL in units of mL) in MCI and AD groups (*P* 0.002) compared with controls. Note there was no significant difference of WMLL between MCI and early AD group. The boxes have lines at the lower quartile (horizontal blue lines), median (horizontal red lines), and upper quartile values. The whiskers are lines extending from each end of the boxes to show the extent of the rest of the data.

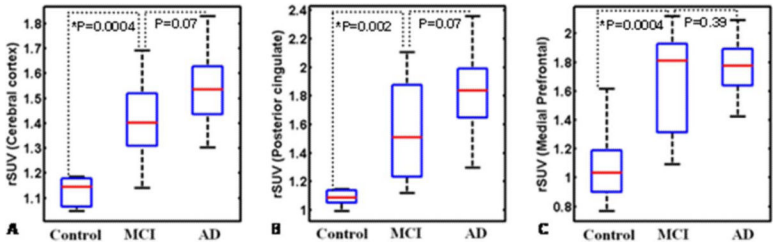

Figure 3.

Increased amyloid uptake measured as ratio of SUV (rSUV) over the referenced cerebellum region in MCI and AD groups compared with controls in the whole cerebral cortex (P = 0.0004) (**A**), posterior cingulate cortex (P = 0.002) (**B**), and medial prefrontal cortex (P = 0.004) (**C**). The boxes have lines at the lower quartile (horizontal blue lines), median (horizontal red lines), and upper quartile values. The whiskers are lines extending from each end of the boxes to show the extent of the rest of the data.

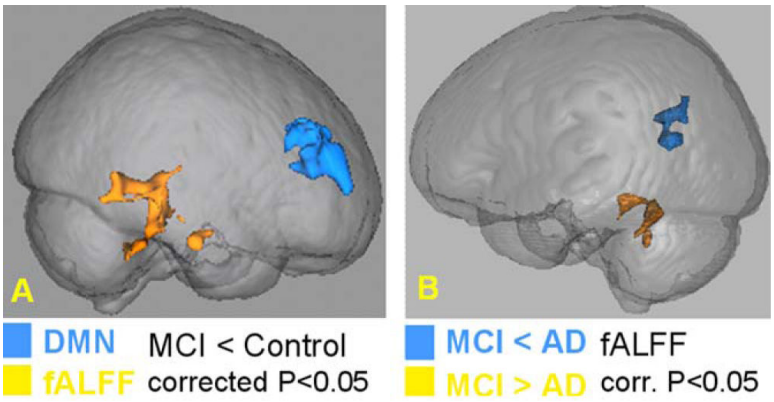

Figure 4.

A: Significantly reduced DMN connectivity in the medial prefrontal area and reduced fALFF activity in the temporal cortex in MCI group compared with control group (Gaussian random field theory, minimum $z > 2.3$, cluster corrected $P < 0.05$). **B:** fALFF was reduced in the temporal cortex but increased in the parietal cortex in patients with AD compared with MCI (corrected $P < 0.05$).

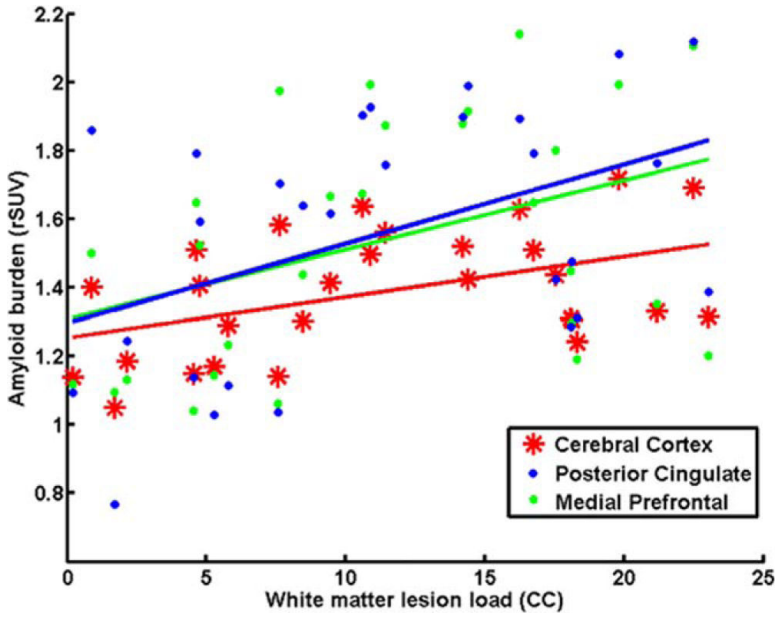

Figure 5.

There was significant correlation between white matter lesion load (WMLL) and amyloid load averaged over the whole brain cerebral cortex in all three groups, shown in red color (Pearson *r* = 0.46; *P* 0.015; Spearman rank *r* = 0.46; *P* = 0.013). There were also significant correlations between WMLL and amyloid load in the posterior cingulate cortex (Pearson r = 0.4; *P* = 0.04; Spearman rank r 0.43; *P* = 0.023) shown in blue color, as well as in the medial pre-frontal cortex (Pearson r = 0.45; *P* 0.018, Spearman rank r = 0.43; *P* ¼ 0.023) (green color).

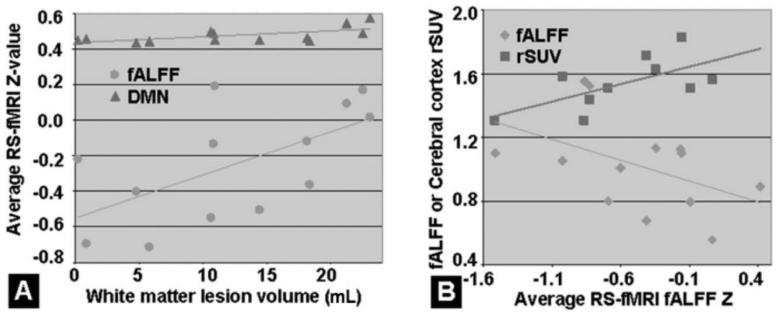

Figure 6.

A: In MCI patients, a significant correlation was found between WMLL and RS-fMRI DMN connectivity strength (i.e., average Z) over the reduced regions (i.e., reduced medial prefrontal cortex connectivity in MCI patients compared with controls) (r = 0.56; *P* = 0.02). Furthermore, there was also a significant correlation between WMLL and RS-fMRI fALFF average *Z* over the reduced regions (i.e., reduced temporal cortex activity in MCI patients compared with controls) (r = 0.63; *P* = 0.01). **B:** In AD patients, a marginal interregional correlation exists between the fALFF activity values (i.e., average *Z* values) over the reduced regions (i.e., decreased medial prefrontal cortex activity in AD patients compared with MCI patients) and increased regions (i.e., increased parietal cortex activity in AD patients compared with MCI patients) (r = 0.46; *P* = 0.11); and a significant correlation was found between amyloid load (rSUV) over the whole cerebral cortex and fALFF activity over the reduced regions (r = 0.64; *P* = 0.046) in AD patients.

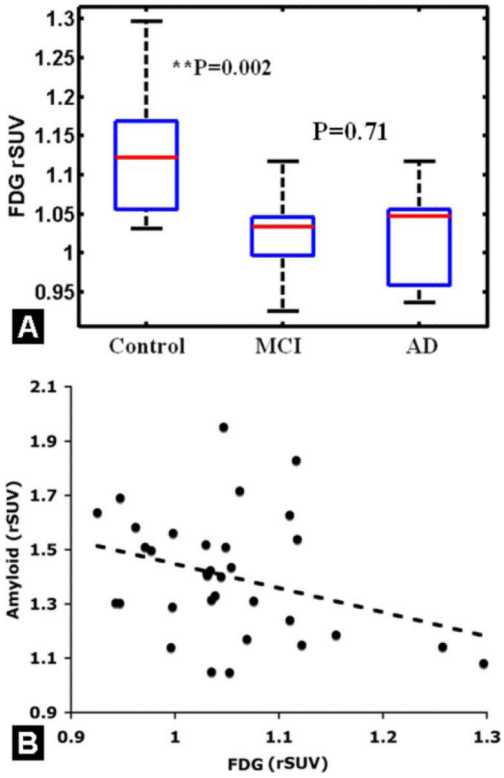

Figure 7.

A: Compared with controls, there was significantly decreased whole brain FDG uptake (rSUV) in MCI and AD groups (*P* = 0.002) compared with controls. Note there was no significant difference of FDG rSUV between MCI and early AD group (*P* 0.71). There was significant correlation between FDG uptake and amyloid load averaged over the whole brain cerebral cortex in all three groups, shown in **B** (Pearson correlation r = 0.57; *P* ¼ 0.0006).

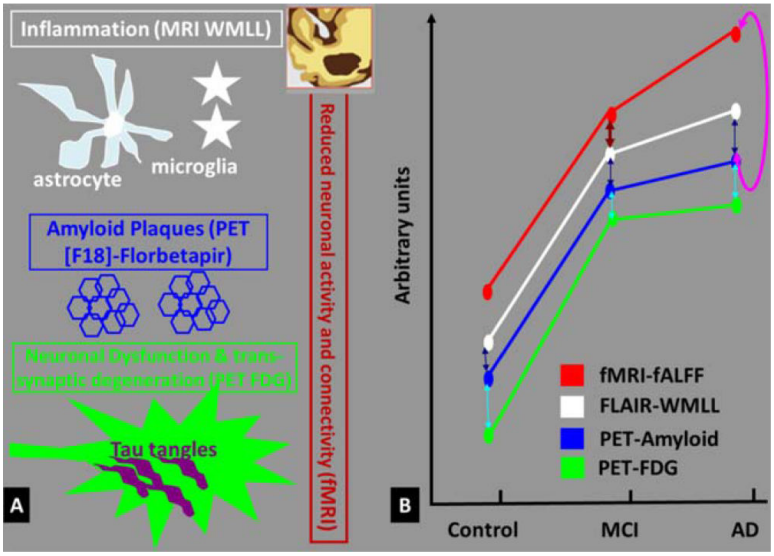

Figure 8.

A: Illustration of spatial correspondence among extracellular white matter inflammation, extracellular amyloid plaques, neuronal and trans-synaptic dysfunction (hypo-metabolism), and neurodegeneration (i.e., reduced neuronal activity) in early AD. **B:** Summary of results suggesting dynamic changes and correlations among four metrics from control to MCI to AD. The WMLL and amyloid deposition were significantly higher in AD and MCI patients compared to controls ($P < 0.05$), with a trend of higher degree in AD compared with MCI. The FDG uptake was lower in AD and MCI compared with controls ($P < 0.002$). The functional activity and connectivity was lower in MCI and AD compared with controls, while there was both decreased and increased functional activity in AD compared with MCI patients. Arrows indicate significant correlations ($P < 0.05$) between metrics within group: WMLL and fALFF in MCI group (purple arrow), amyloid and fALFF in AD group (red arrow), WMLL and amyloid load (all groups, blue), FDG uptake and amyloid load (all groups, cyan).

Table 1

Demographics of Downloaded ADNI Data With Means and SDs of Age, MMSE, CDR, and Gender Information

Group	Control	MCI	AD
No. of Subjects	14	17	13
Age (y)	76.3±8.3	76.7±5.5	76.2±8.4
Female, %	64%	53%	62%
Male, %	36%	47%	38%
MMSE	29.2±0.4	26.1±0.7	22.3±1.7
CDR	0.0±0.0	0.5±0.1	1.0±0.1